Accepted Manuscript online: 2022-10-04 Article published online: 2022-10-28

Emission-Tunable and Elastically Bendable Organic Polymorphs for Lasing Media

Baolei Tang[a]
Shiyue Tang[a]
Kaiqi Ye[a]
Hongyu Zhang* [a]

[a] State Key Laboratory of Supramolecular Structure and Materials, College of Chemistry, Jilin University, Changchun 130012, P. R. of China

* hongyuzhang@jlu.edu.cn

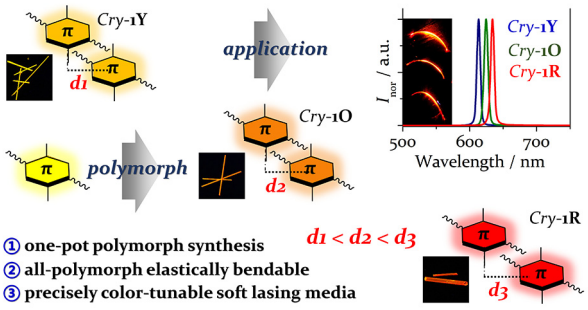

Received: 02.09.2022
Accepted after revision: 29.09.2022
DOI: 10.1055/a-1954-3823; Art ID: OM-2022-09-0036-SC

Abstract Crystal engineering has served as a powerful strategy to grow organic molecular crystals with different physical behaviors and this strategy has been also attempted for a purpose to grow crystals with desired mechanical properties; however, it is quite challenging to endow all different crystal phases constructed by the same compound with unique reversible deformation, such as elastic bending. We herein report a rare example of all-polymorph elastic crystals accompanied by precisely tunable emission colors. Single-crystal structure analyses and their optical and mechanical properties have been fully investigated on all polymorphs. The color-tunable amplified spontaneous emissions of both the straight and elastically bent polymorphs demonstrate the applicability of these elastic polymorphs in future wearable optoelectronic devices.

Key words: organic polymorphs, crystal structures, elastic deformation, mechanical properties, amplified spontaneous emission

Introduction

Natural crystals are the materials known to the ancient world, and the term “crystal” is derived from the Ancient Greek word “κρύσταλλος (krustallos)”, meaning both ice and rock.[1] The definition clearly describes two natures of crystalline materials, namely, hardness and brittleness. Crystals have been widely used in human daily life for thousands of years even though their accurate structures were not clear until the last century. At the beginning of the 20th century, the great scientist W. L. Bragg discovered the single-crystal X-ray diffraction (SCXRD) technology, which could accurately determine the molecular structure at the atomic level.[2] After that, crystallography has forever marked its position in science and developed vigorously as reflected by the spewing crystal structures deposited in the Cambridge Structural Database. Among various crystalline materials, molecular crystals with optical functions have attracted great attention due to their intriguing natures such as long-range ordered packing structures, anisotropic physical properties, intense emissions, high charge transporting abilities, etc.[3–7] Although organic crystals show significant shortcomings when compared with plastics, the dynamic adaptive ability in the long-range ordered structure, light weight, low cost, and unique anisotropic physical properties of organic crystals have placed them as potential alternative materials for applications in optoelectronics.

Recently, a number of dynamic adaptive organic molecular crystals have been designed with extreme novel capabilities, including bending,[8–13] twisting,[14–17] curling,[18,19] and even of shape memory effect.[20,21] Shape transformation of single crystals by external stimuli such as heat, light, humidity, and external force has been extensively studied.[9,22–27] Compared with the huge amounts of molecular crystals, those with deformation abilities (elasticity and/or plasticity) are extremely rare. Moreover, most of the flexible organic crystals reported so far are obtained occasionally or based on the trial-and-error method. Thus, improving the odds of constructing organic crystals with desired flexibilities is pivotal in advancing the newly shaped research direction of mechanically compliant organic crystals. Crystal engineering has served as a powerful strategy to grow crystals with different physical behaviors, based on which abundant organic polymorphs with tunable emission colors have been reported.[28–30] In addition, several molecular crystals with deformation abilities in response to external stresses were realized through screening crystallization conditions.[31–33] For instance, based on a simple diketone molecule, we obtained three polymorphs which exhibited quite different mechanical properties of brittleness, elasticity and plasticity.[34–37] This strategy has been attempted on other

molecular systems for a purpose to grow crystals with desired mechanical properties; however, it is quite challenging to endow all different crystal phases constructed by the same compound with unique reversible deformation ability. In this sense, it would be fascinating if the polymorphs of an organic emitter can exhibit tunable emission colors and at the same time they all possess elastically bendable ability.

We herein report an example to elucidate that the as-mentioned problem might be solvable by molecular design together with polymorph engineering. A single-benzene molecule **1** was designed for this purpose following the considerations of: (1) the compact π-system is an ideal unit for designing a red emitter, (2) the flat and rigid framework possesses high crystallinity, and (3) the side chains form rich intermolecular interactions, beneficial for the generation of polymorphs. Three organic crystals (*Cry*-**1Y**, *Cry*-**1O**, and *Cry*-**1R**) with tunable emissions are obtained, and they exhibit reversible bending–relaxing deformations upon applying and releasing external forces. Thus, organic polymorphs with elastically deformable capabilities as well as tunable emission colors are achieved for the first time. The optical properties and mechanical behaviors of *Cry*-**1Y**, *Cry*-**1O**, and *Cry*-**1R** have been fully investigated. SCXRD analyses have been carried out to provide insights into the critical roles of molecular packing and intermolecular interactions in optimizing optical and mechanical properties. Finally, the superiority of elastic deformation and emission adjustability of these polymorphs have been highlighted by evaluating the crystal lasing potentials in both the straight and bent states.

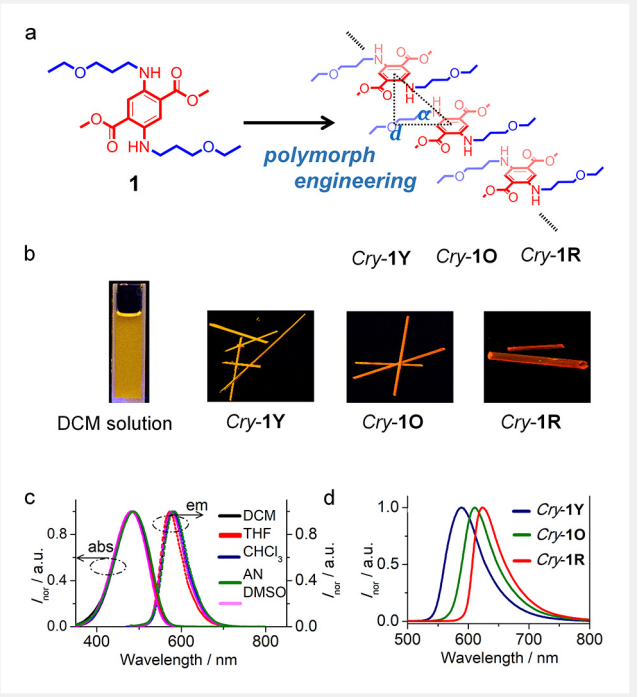

Figure 1 Chemical structure of molecule **1** and molecular columns in crystals **1Y**, **1O** and **1R** obtained by polymorph engineering (a), photographic images of DCM solution samples, *Cry*-**1O**, *Cry*-**1Y**, and *Cry*-**1R**, under 365 nm UV irradiation (b), absorption and emission spectra of **1** in different solvents (c), and emission spectra of the crystalline samples (d).

Results and Discussion

The title compound **1** (Figure 1a) was synthesized through a one-step reaction in high isolated yield (76%). The target was fully characterized by ^{1}H and ^{13}C NMR, elemental analysis and mass spectrometry. Three polymorphs, *Cry*-**1Y** (yellow), *Cry*-**1O** (orange), and *Cry*-**1R** (red), with similar needle-like shape were obtained simultaneously in the same test tube or flask by a solution diffusion of methanol into dichloromethane (DCM) solution containing **1**. Different crystals could be easily recognized and separated due to their visually distinguishable colors and emissions. ^{1}H NMR spectra of *Cry*-**1Y**, *Cry*-**1O**, and *Cry*-**1R** were measured and compared to confirm that the difference among these crystals is solely originated from the molecular arrangements. Compound **1** emitted orange fluorescence in DCM (Figure 1b) with moderate quantum yield ($\Phi = 0.36$). The absorption and emission spectra of **1** in various solutions are depicted in Figure 1c, demonstrating that the polarity of solutions has little effect on both the ground and excited states. The emissions of *Cry*-**1Y**, *Cry*-**1O**, and *Cry*-**1R** are different (Figure 1d), being at 588 nm ($\Phi = 0.49$), 610 nm ($\Phi = 0.29$), and 624 nm ($\Phi = 0.18$), respectively. Thus, the emissions of *Cry*-**1Y**, *Cry*-**1O**, and *Cry*-**1R** are polymorph-dependent.

All crystals display elastic bending deformations when transverse forces were applied on the wide surface, as shown in Figure 2a, 2c, and 2e. Taking *Cry*-**1Y** as an example, the straight crystal gradually bent into a half loop when a needle was pressed on the central part against a pair of forceps. After releasing the pressure, it recovered the original straight shape immediately without any fracture. Repeated bending–relaxing cycles were carried out on the identical crystal. The crystal maintained the smooth surface in the bent states as reflected by scanning electron microscopy (SEM) images. Over-bending of the crystal resulted in the breakage without plastic deformation. The other two polymorphs, *Cry*-**1O** and *Cry*-**1R**, exhibited similar elastic bending processes to *Cry*-**1Y**, as shown in Figure 2c and 2e. To confirm the elastic nature of *Cry*-**1Y**, *Cry*-**1O**, and *Cry*-**1R**, three-point bending experiments were carried out and the stress–strain curves are outlined in Figure 2b, 2d, and 2f, respectively. The morphologies and schematic diagrams of the cross-sections of *Cry*-**1Y**, *Cry*-**1O**, and *Cry*-**1R** are shown in Figure 2g–i. In order to ensure the reliability of the data, three different crystals of *Cry*-**1Y**, *Cry*-**1O**, and *Cry*-**1R** were subjected to these measurements. The linear shape of the

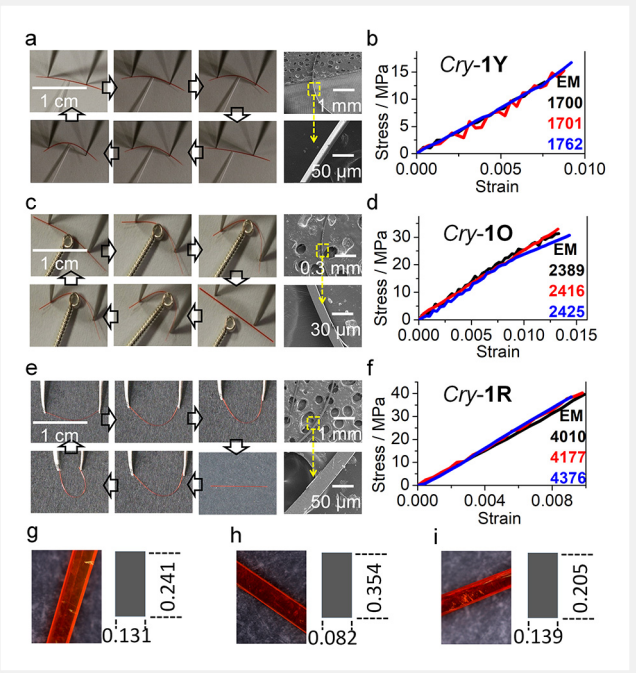

Figure 2 The bending–relaxing process and SEM images of *Cry*-**1Y** (a), *Cry*-**1O** (c), and *Cry*-**1R** (e), strain–stress curves of *Cry*-**1Y** (b), *Cry*-**1O** (d), and *Cry*-**1R** (f), and the images of the bendable crystal surfaces and the cross-section sizes of *Cry*-**1Y** (g), *Cry*-**1O** (h), and *Cry*-**1R** (i). (For mechanical property measurements, three different samples were tested for all polymorphs.)

stress–strain curves indeed confirmed the intrinsic elasticity of these polymorphs. The average elastic moduli were calculated to be 1.72, 2.40, and 4.18 GPa for *Cry*-**1Y**, *Cry*-**1O**, and *Cry*-**1R**, respectively, which are at the average range of other organic elastic crystals.[38–40] In addition, the average fracture strengths were determined to be 15.05, 31.64, and 39.50 MPa for *Cry*-**1Y**, *Cry*-**1O**, and *Cry*-**1R**, respectively.

These polymorphs are featured with elastically bendable behaviors and tunable emission colors are a rare case in engineering mechanical properties of organic crystals. Hence, SCXRD analyses of *Cry*-**1Y**, *Cry*-**1O**, and *Cry*-**1R** were carried out to provide the detailed information of molecular conformations, packing structures, and intermolecular interactions. It is interesting to find that *Cry*-**1Y**, *Cry*-**1O**, and *Cry*-**1R** belong to the same triclinic system as well as the *P*-1 space group despite having different cell parameters (Table S1). Only one individual molecule exists in the unit cell in all polymorphs (Figure 3a). They adopt rather flat and rigid skeletons at the central part, including the benzene ring, ester groups, and the NH moieties, due to the strong intramolecular H-bonds with a H—O distance of 2.066, 2.039, and 2.043 Å for *Cry*-**1Y**, *Cry*-**1O**, and *Cry*-**1R**, respectively (Figure S1). The side chains spread out and deviate from the benzene plane, and the deviation degrees are slightly different among these polymorphs, as shown in Figures 3b and S2.

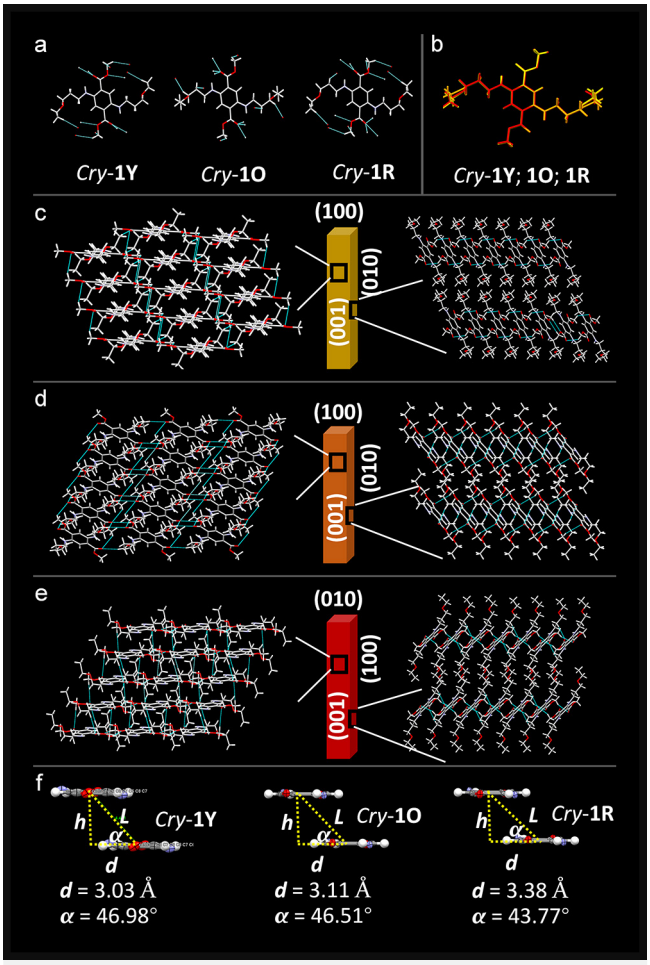

Figure 3 Individual molecular structures of *Cry*-**1O**, *Cry*-**1Y**, and *Cry*-**1R** (a), the overlapped structures showing the conformation difference (b), molecular packing structures of *Cry*-**1Y** in the (001) and (010) planes (c), molecular packing structures of *Cry*-**1O** in the (001) and (010) planes (d), molecular packing structures of *Cry*-**1R** in the (001) and (100) planes (e), and the *J*-type aggregation degree between neighboring molecules within the column structures of *Cry*-**1O**, *Cry*-**1Y**, and *Cry*-**1R** (f). (Blue dotted lines: intermolecular hydrogen bonds; *l*: the distance between two centroids of the benzene ring; *h*: the vertical distance between two molecules; *d* and *α*: the calculated distance and one of the acute angles of the yellow right triangle)

Owing to the presence of the C=O and NH as well as ether oxygen moieties, there are rich intermolecular H-bonds between neighboring molecules, which affect the molecular arrangements. Although the spatial locations of side chains are different, the number (12 for each molecule) and strength (H—O distance: 2.537–2.697 Å for *Cry*-**1Y**; 2.487–2.751 Å for *Cry*-**1O**; and 2.514–2.708 Å for *Cry*-**1R**) of intermolecular H-bonds in *Cry*-**1Y**, *Cry*-**1O**, and *Cry*-**1R** are quite similar (Figure S3).

For *Cry*-**1Y**, expanding these H-bonds generates an infinite supramolecular layer structure in the crystallographic

(001) plane (Figure 3c), which is determined to be the bendable plane by face indexing (Figure S4a). Within the (001) plane, there exist π-stacked molecular columns along the crystallographic [100] direction (crystal growth direction). The H-bonded molecular layers stacked along the [001] direction through van der Waals forces between side chains, forming the (010) plane that is perpendicular to (001). The π-stacked columns expanded or compressed accompanied by certain rotations of individual molecules in response to external stress, resulting in the macroscopic elastic deformation. As shown in Figure 3d, intermolecular H-bonds in *Cry*-**1O** drive the formation of the bendable (001) plane (Figure S4b) that stacks parallelly and forms the (010) plane. In the bendable plane, the π-stacked molecular columns along the crystal growth [100] direction are mainly responsible for absorbing and releasing energy during the bending–relaxing process in response to external force. The van der Waals forces between side chains together with molecular rotations also contribute to the macroscopic elastic bending of the bulk crystals. The bendable plane in *Cry*-**1R** is determined to be (001) by face indexing (Figure S4c), in which the molecules are connected through 12 intermolecular H-bonds as mentioned above. The crystal growth direction in *Cry*-**1R** is different to that in *Cry*-**1Y** and *Cry*-**1O**, being π-stacked molecular columns are formed along [010]. Thus, the molecular arrangements in the (100) plane are important in terms of the mechanical properties of *Cry*-**1R**. As shown in Figure 3e, the π-stacked molecular columns along the [010] direction are interacted through van der Waals forces between side chains. It is reasonable to consider that the crystal displays macroscopic elastic bending when a transverse force was applied on the (001) plane. Based on these structural analyses, the relatively constant intermolecular H-bonds as well as the rigid core structure are the footing stone of the elastic deformation of these polymorphs, and the variable spatial location of the side chains is crucial for the generation of polymorphs.

Considering the very similar crystal structures, the emission difference among *Cry*-**1Y**, *Cry*-**1O**, and *Cry*-**1R** is quite interesting. To make this point clear, we further carefully compared the π-stacked structures of these polymorphs. The emissive units of the central benzene skeleton are stacked parallel with large slip angles, which implies the molecules adopt a *J*-type aggregation. According to the Kasha rule, *J*-aggregation usually causes red-shifted emission of organic dyes. As shown in Figure 3f, a molecular dimer was employed to show the degree of molecular overlap. The distance between centroids of neighboring benzenes and the vertical distance between benzenes within the dimer are denoted as *l* and *h*, respectively. While *d* and *α* are the calculated distance and one acute angle, respectively, based on the formula of the Pythagorean theorem. The *d* values are in the order of 3.03 Å (*Cry*-**1Y**) < 3.11 Å (*Cry*-**1O**) < 3.38 Å (*Cry*-**1R**), whereas the *α* values are in the opposite trend of 46.98° (*Cry*-**1Y**) > 46.51° (*Cry*-**1O**) > 43.77° (*Cry*-**1R**). These two trends clearly demonstrate that the overlap degree of two neighboring molecules is in the order of *Cry*-**1Y** < *Cry*-**1O** < *Cry*-**1R**. Thus, the degree of *J*-aggregation component in the molecular packing structures is *Cry*-**1Y** < *Cry*-**1O** < *Cry*-**1R**, consistent with the emission maximum trend of 588 nm (*Cry*-**1Y**) < 610 nm (*Cry*-**1O**) < 624 nm (*Cry*-**1R**). Hence, the spatial position of carbon chains precisely modulates the *J*-aggregation component and thereby the emission colors of the bulky samples.

The high-quality polymorphs with smooth surface and needle-like morphology show higher emission intensity at the tips than at the body under 365 nm UV light irradiation, indicating that the light was confined inside the crystal and propagated along the body efficiently. Then, the optical functions of these elastic bending polymorphs were checked by measuring the amplified spontaneous emissions (ASEs) at both the straight and bent states (Figure 4a,b).[41] The straight and bent crystals of *Cry*-**1Y** were irradiated by a pump laser beam (355 nm, 10 Hz) at the central part, and the stimulated light at one tip was recorded using a Maya2000 Pro CCD spectrometer. Upon increasing the pump energy over a certain degree, the detected emission spectra significantly narrowed accompanied by suddenly enhanced intensities. The energy-dependent emission intensity and full width at half maximum (FWHM) shown in Figure 4c and 4d clearly demonstrate that the straight and elastically bent crystals are ASE-active. The other two polymorphs *Cry*-**1O** and *Cry*-**1R** display similar ASE behaviors to *Cry*-**1Y**, as shown in Figure S5. The narrowest FWHM is determined to be 6, 7, and 7 nm in the straight state and 8, 7, and 9 nm for the bent crystals of *Cry*-**1Y**, *Cry*-**1O**, and *Cry*-**1R**, respec-

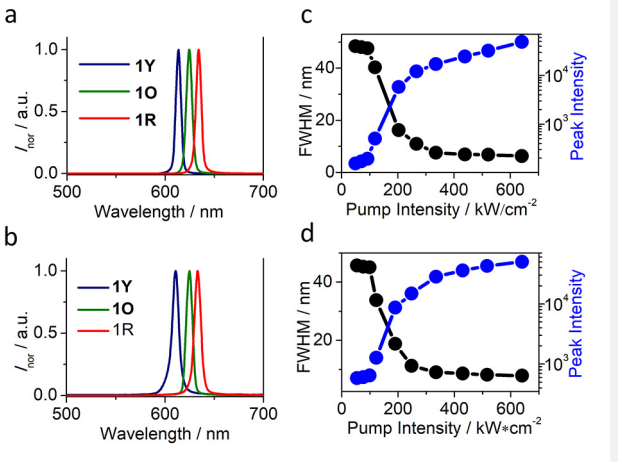

Figure 4 The narrowest ASE spectra of the straight crystals *Cry*-**1O**, *Cry*-**1Y**, and *Cry*-**1R** (a), the narrowest ASE spectra of the elastically bent crystals *Cry*-**1O**, *Cry*-**1Y**, and *Cry*-**1R** (b), and dependence of peak intensity and FWHM of the emission bands of the straight (c) and bent (d) crystals of **1Y**.

tively. The narrowed emissions were located in the deep red region with CIE coordinates of (0.67, 0.33) for *Cry*-**1Y**, (0.69, 0.31) for *Cry*-**1O**, and (0.71, 0.29) for *Cry*-**1R** (Figure S6). The significant redshifts of stimulated emissions compared with the fluorescence are due to the reabsorption during the long-range light propagation along the crystal body. It is worth noting that these polymorphs also show different ASE peaks in both the straight (613, 624, and 634 nm for *Cry*-**1Y**, *Cry*-**1O**, and *Cry*-**1R**, respectively) and the bent states (610, 620, and 630 nm for *Cry*-**1Y**, *Cry*-**1O**, and *Cry*-**1R**, respectively). Thus, the precise tuning of ASE color of flexible crystals has been achieved by polymorph engineering.

Conclusions

In summary, we report a rare example of elastically bendable organic polymorphs with precisely tunable emissions without even screening crystallization conditions based on a single-benzene emitting framework. The superiority of the elastic deformation capabilities and emission adjustability of these polymorphs has been highlighted by evaluating the crystal lasing potentials in both the straight and bent states. This study provides a possible guide to design polymorph-dependent emissions of organic crystals with inherent elastic deformations which can be hardly achieved via a common crystal engineering strategy. The proposed polymorph engineering strategy is now expanding for growing organic crystals with invariable flexibility but with tunable emissions based on other highly emissive organic dyes, and these works are currently in progress in our laboratory.

Funding Information

This work was supported by the National Natural Science Foundation of China (Grant Number 52 173 164).

Supporting Information

Supporting Information for this article is available online at https://doi.org/10.1055/a-1954-3823.

Conflict of Interest

The authors declare no conflict of interest.

References and Notes

(1) Nesse, W. D. *Introduction to Mineralogy*, Oxford University Press: New York, 1999.
(2) Bragg, W. H. *Nature*, **1912**, *90*, 360.
(3) Zhang, C.; Zhao, Y. S.; Yao, J. *Phys. Chem. Chem. Phys.* **2011**, *13*, 9060.
(4) Zhang, W.; Yan, Y.; Gu, J.; Yao, J.; Zhao, Y. S. *Angew. Chem. Int. Ed.* **2015**, *54*, 7125.
(5) Wang, Y.; Wu, H.; Zhu, W.; Zhang, X.; Liu, Z.; Wu, Y.; Feng, C.; Dang, Y.; Dong, H.; Fu, H.; Hu, W. *Angew. Chem. Int. Ed,* **2021**, *60*, 6344.
(6) Liu, D.; Liao, Q.; Peng, Q.; Gao, H.; Sun, Q.; De, J.; Gao, C.; Miao, Z.; Qin, Z.; Yang, J.; Fu, H.; Shuai, Z.; Dong, H.; Hu, W. *Angew. Chem. Int. Ed.* **2021**, *60*, 20274.
(7) Lv, Z.; Man, Z.; Xu, Z.; Fu, L.; Li, S.; Zhang, Y.; Fu, H. *Adv. Opt. Mater.* **2021**, *9*, 2100598.
(8) Ghosh, S.; Reddy, C. M. *Angew. Chem. Int. Ed.* **2012**, *51*, 10319.
(9) Ahmed, E.; Karothu, D. P.; Naumov, P. *Angew. Chem. Int. Ed.* **2018**, *57*, 8837.
(10) Annadhasan, M.; Karothu, D. P.; Chinnasamy, R.; Catalano, L.; Ahmed, E.; Ghosh, S.; Naumov, P.; Chandrasekar, R. *Angew. Chem. Int. Ed.* **2020**, *59*, 13821.
(11) Annadhasan, M.; Agrawal, A. R.; Bhunia, S.; Pradeep, V. V.; Zade, S. S.; Reddy, C. M.; Chandrasekar, R. *Angew. Chem. Int. Ed.* **2020**, *59*, 13852.
(12) Hayashi, S.; Ishiwari, F.; Fukushima, T.; Mikage, S.; Imamura, Y.; Tashiro, M.; Katouda, M. *Angew. Chem. Int. Ed.* **2020**, *59*, 16195.
(13) Hayashi, S.; Koizumi, T. *Chem. Eur. J.* **2018**, *24*, 8507.
(14) Catalano, L.; Karothu, D. P.; Schramm, S.; Ahmed, E.; Rezgui, R.; Barber, T. J.; Famulari, A.; Naumov, P. *Angew. Chem. Int. Ed.* **2018**, *57*, 17254.
(15) Liu, H.; Lu, Z.; Tang, B.; Qu, C.; Zhang, Z.; Zhang, H. *Angew. Chem. Int. Ed.* **2020**, *59*, 12944.
(16) Saha, S.; Desiraju, G. R. *Chem. Commun.* **2017**, *53*, 6371.
(17) Saha, S.; Desiraju, G. R. *J. Am. Chem. Soc.* **2017**, *139*, 1975.
(18) Kim, T.; Al-Muhanna, M. K.; Al-Suwaidan, S. D.; Al-Kaysi, R. O.; Bardeen, C. J. *Angew. Chem. Int. Ed.* **2013**, *52*, 6889.
(19) Wang, H.; Chen, P.; Wu, Z.; Zhao, J.; Sun, J.; Lu, R. *Angew. Chem. Int. Ed.* **2017**, *56*, 9463.
(20) Ahmed, E.; Karothu, D. P.; Warren, M.; Naumov, P. *Nat. Commun.* **2019**, *10*, 3723.
(21) Chung, H.; Dudenko, D.; Zhang, F.; D'Avino, G.; Ruzie, C.; Richard, A.; Schweicher, G.; Cornil, J.; Beljonne, D.; Geerts, Y.; Diao, Y. *Nat. Commun.* **2018**, *9*, 278.
(22) Good, J. T.; Burdett, J. J.; Bardeen, C. J. *Small* **2009**, *5*, 2902.
(23) Halabi, J. M.; Ahmed, E.; Catalano, L.; Karothu, D. P.; Rezgui, R.; Naumov, P. *J. Am. Chem. Soc.* **2019**, *141*, 14966.
(24) Karothu, D. P.; Mahmoud Halabi, J.; Li, L.; Colin-Molina, A.; Rodriguez-Molina, B.; Naumov, P. *Adv. Mater.* **2020**, *32*, 1906216.
(25) Liu, H.; Ye, K.; Zhang, Z.; Zhang, H. *Angew. Chem. Int. Ed.* **2019**, *58*, 19081.
(26) Lu, Z.; Zhang, Y.; Liu, H.; Ye, K.; Liu, W.; Zhang, H. *Angew. Chem. Int. Ed.* **2020**, *59*, 4299.
(27) Nath, N. K.; Pejov, L.; Nichols, S. M.; Hu, C.; Saleh, N.; Kahr, B.; Naumov, P. *J. Am. Chem. Soc.* **2014**, *136*, 2757.
(28) Wang, L.; Wang, K.; Zou, B.; Ye, K.; Zhang, H.; Wang, Y. *Adv. Mater.* **2015**, *27*, 2918.
(29) Yan, D.; Evans, D. G. *Mater. Horiz.* **2014**, *1*, 46.
(30) Zhen, Y. G.; Dong, H. L.; Jiang, L.; Hu, W. P. *Chin. Chem. Lett.* **2016**, *27*, 1330.
(31) Cao, L.; Tang, B.; Yu, X.; Ye, K.; Zhang, H. *CrystEngComm* **2021**, *23*, 5758.
(32) Chu, X.; Lu, Z.; Tang, B.; Liu, B.; Ye, K.; Zhang, H. *J. Phys. Chem. Lett.* **2020**, *11*, 5433.

(33) Liu, B.; Di, Q.; Liu, W.; Wang, C.; Wang, Y.; Zhang, H. *J. Phys. Chem. Lett.* **2019**, *10*, 1437.
(34) Huang, R.; Tang, B.; Ye, K.; Wang, C.; Zhang, H. *Adv. Opt. Mater.* **2019**, *7*, 1900927.
(35) Huang, R.; Wang, C.; Wang, Y.; Zhang, H. *Adv. Mater.* **2018**, *30*, 1800814.
(36) Liu, B.; Lu, Z.; Tang, B.; Liu, H.; Liu, H.; Zhang, Z.; Ye, K.; Zhang, H. *Angew. Chem. Int. Ed.* **2020**, *59*, 23117.
(37) Tang, B.; Liu, B.; Liu, H.; Zhang, H. *Adv. Funct. Mater.* **2020**, *30*, 2004116.
(38) Tang, S.; Ye, K.; Zhang, H. *Angew. Chem. Int. Ed.* **2022**, *61*, e202210128.
(39) Di, Q.; Miao, X.; Lan, L.; Yu, X.; Liu, B.; Yi, Y.; Naumov, P.; Zhang, H. *Nat. Commun.* **2022**, *13*, 5280.
(40) Chao, J.; Liu, H.; Zhang, H. *CCS Chem.* **2020**, *2*, 2569.
(41) The crystal was irradiated by the third harmonic (355 nm) of a Nd : YAG laser at a repetition rate of 10 Hz and a pulse duration of about 10 ns. The energy of the pumping laser was adjusted by using the calibrated neutral density filters. The beam was focused into a stripe whose shape was adjusted to 3.3 × 0.6 mm^2 by using a cylindrical lens and a slit. The edge emission and PL spectra of the crystals were detected using a Maya2000 Pro CCD spectrometer.